Surface plasmon and electron–hole structures in the excitation spectra of thin films

2006 J. Phys.: Condens. Matter 18 4253

(http://iopscience.iop.org/0953-8984/18/17/013)

INSTITUTE OF PHYSICS PUBLISHING JOURNAL OF PHYSICS: CONDENSED MATTER

J. Phys.: Condens. Matter **18** (2006) 4253–4263 doi:10.1088/0953-8984/18/17/013

Surface plasmon and electron–hole structures in the excitation spectra of thin films

L Marušić[1], **V Despoja and M Šunjić**

Department of Physics, University of Zagreb, Bijenička 32, HR-10000, Zagreb, Croatia

E-mail: leo@phy.hr

Received 20 January 2006, in final form 22 March 2006
Published 13 April 2006
Online at stacks.iop.org/JPhysCM/18/4253

Abstract

Surface excitation spectra are calculated, including both collective and single-particle modes, and examined in detail. This is achieved by calculating the non-local dielectric function $\varepsilon_p(\mathbf{Q}, z, z', \omega)$ of the thin jellium film within the random phase approximation (RPA) (using local density approximation wavefunctions which actually takes us beyond the RPA), from which we then derive the spectral function. The high precision of the calculations enables us to analyse not only the collective (surface plasmon) modes and their dependence on the film thickness, but also the intra-band electron–hole excitations, and for the first time oscillatory structures due to inter-band transitions. The spectra are then analysed with special attention to their dependence on the slab thickness, and the periodic peaks observed due to single-particle excitations in the spectra.

1. Introduction

It is well known that the bulk excitations in a metallic slab practically do not produce electric fields outside the metal because they are almost completely screened. Therefore, in order to calculate the fields experienced by a charged particle placed outside the metal, it is necessary to study the surface excitations (collective and single particle) in detail. Such calculations have been performed by a number of authors [1–23] for various systems and geometries, not only for a metallic slab but also for semi-infinite metal and metal–vacuum–metal systems. The results have a wide relevance and they have for example been applied to studies of the energy loss in EELS (electron energy loss spectra) experiments, electron tunnelling in semiconductor heterostructures or in STM (scanning tunnelling microscope), calculations of surface states, etc. In processes where particles are close to the surface, or in systems like thin metallic slabs or metallic electrodes separated by a narrow gap (as is the case in STM) the electrons are very close to the surface, so both single-particle and collective excitations

[1] Present address: Department of Transport and Maritime Studies, University of Zadar, R Boškovića 5, HR-23000, Zadar, Croatia.

have to be taken into account, instead of limiting the calculations to the collective modes in the long-wavelength limit. This can be achieved by deriving the relation between the non-local interaction propagator $W(\mathbf{r}, \mathbf{r}', \omega)$, and the non-local dielectric function $\varepsilon(\mathbf{r}, \mathbf{r}', \omega)$ (or polarizability $\widetilde{\chi}(\mathbf{r}, \mathbf{r}', \omega)$), and calculating the dielectric function within the random phase approximation (RPA) but using the local density approximation (LDA) [1] wavefunctions (which actually gets us beyond the usual RPA). This approach provides the non-local dielectric function which is not just a tool for the calculation of the screened interaction propagator, but is also very useful in determining for example excitation spectra and dispersion relations.

The relation between the non-local interaction propagator and the dielectric function in this form was first derived by Newns [2], but he only examined in detail the case when points z and z' are both outside the flat metal surface. In our previous work we generalized this method to the case when the surface is not necessarily flat, but of a general curvature [3], and for the flat surface we extended this method to situations where one or both points are inside the metal [4].

To calculate the dielectric function (or to obtain the non-local interaction propagator W) we need to calculate the response function of the metallic slab, and for this we need electron wavefunctions. Since the electrons are very close to the surface one cannot use the free electron or even infinite barrier model (IBM) wavefunctions, but we need more realistic jellium wavefunctions, e.g. Kohn–Sham wavefunctions. They can be obtained by expanding them in terms of sinusoidal IBM wavefunctions and solving a matrix version of the Kohn–Sham [5] problem to obtain the expansion coefficients [6], or by solving the Kohn–Sham equation for the jellium slab numerically [1, 7], as we do here. Our calculation is slightly different from those presented in [1, 7], and is described in detail in [8].

The wavefunctions (and then the response function and the excitation spectra) can also be obtained for more realistic models of a crystal, including for example the surface periodic potential, or more complicated cases, using various *ab initio* methods [9], but then the system is not translationally invariant in the direction parallel to the surface but periodic, and the response function is not be diagonal with respect to the wavevector parallel to the surface $\mathbf{Q}$, i.e. instead of $\chi_{qq'}(\mathbf{Q}, \omega)$, we have $\chi_{qq'}(\mathbf{Q}, \mathbf{G}, \omega)$, which complicates the calculation tremendously. Such calculations were done, for example to obtain a GW correction of the LDA exchange–correlation potential [10], or to calculate the dynamical response and plasmon dispersion for the bulk aluminium [11], and even to examine surface plasmons (SPs) for metal monolayers [12] and a single metal surface [13], but still not for a slab of finite and variable thickness. Since we want to examine the influence of the slab thickness on the excitation spectra we use the jellium model, which has the advantage of being translationally invariant in the direction parallel to the surface, but still enables a relatively realistic description of charge fluctuations. Furthermore, the method we use enables us not just to calculate the total spectra, containing all the excitations in such a slab (as is done in all the aforementioned references based on the *ab initio* calculations), but also to separate and clearly distinguish spectral features due to specific excitations (bulk, surface, odd, even, collective, single particle). Therefore, we study not only the strong surface plasmon peaks and broad structures due to intra-band electron–hole transitions, but also the discrete peaks due to inter-band transitions. We also examine how the peaks in the single-particle excitation spectra are related to the slab thickness and the energy levels of the bound states within the slab.

2. Formulation of the problem

We study a thin metallic slab in a jellium model, with the thickness varying approximately from 10 to 100 atomic units. The slab is infinite in the $\boldsymbol{\rho} = (x, y)$ plane, and finite in the z direction, $-L < z < 0$. We assume that the electron density practically vanishes at the boundaries

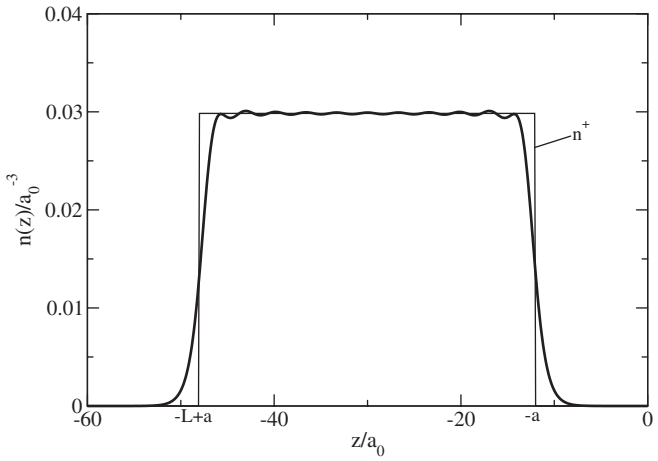

Figure 1. Geometry of the slab, and calculated electron density profile for $r_s = 2.07$. Positive background extends from $-L + a$ to $-a$. $n(z)$ is the electron charge density, and n^+ is the positive background charge density.

$z = -L$ and $z = 0$, with the positive background extending from $z = -L + a$ to $z = -a$, i.e. its thickness is $d = L - 2a$ (figure 1).

Therefore, all quantities could be Fourier transformed in the $\boldsymbol{\rho}$ direction as

$$f(\mathbf{Q}, z, z') = \int_A \mathrm{d}\boldsymbol{\rho} \mathrm{e}^{\mathrm{i}\mathbf{Q}\boldsymbol{\rho}} f(\mathbf{r}, \mathbf{r}') \tag{1}$$

$$f(\mathbf{r}, \mathbf{r}') = \frac{1}{(2\pi)^2} \int \mathrm{d}\mathbf{Q} \mathrm{e}^{-\mathrm{i}\mathbf{Q}\boldsymbol{\rho}} f(\mathbf{Q}, z, z') \tag{2}$$

where A is the total surface of the metal and $\mathbf{Q}$ is a wavevector parallel to the surface.

The wavefunctions can be written in the form

$$\Phi_\nu(\mathbf{r}) = \sqrt{\frac{2}{AL}} \mathrm{e}^{\mathrm{i}\mathbf{Q}\boldsymbol{\rho}} \phi_n(z) \tag{3}$$

where $\nu = (\mathbf{Q}, n)$ and $\phi_n(z)$ is the self-consistent solution of the one-dimensional Kohn–Sham equation for the jellium slab. The corresponding energies can be written as

$$E_n = \frac{\hbar^2 Q^2}{2m} + \epsilon_n \tag{4}$$

where m is the electron mass and ϵ_n is the 'perpendicular' part of the energy, i.e. the eigenvalue obtained by the solution of the one-dimensional Kohn–Sham equation.

Since our slab is symmetrical with respect to the $z = -L/2$ plane, we can decompose the charge fluctuation modes into symmetric ($p = +$) and antisymmetric ($p = -$) ones. Moreover, since in the linear response theory (anti)symmetric modes couple only with (anti)symmetric external perturbations, it is convenient to decompose our potentials into symmetric and antisymmetric parts, and treat them separately. That way our system will always have a well defined symmetry, making it plausible to perform Fourier transforms in the z direction using the (anti)symmetrical functions

$$f_q^p = \int_{-L}^{0} \mathrm{d}z\, f(z) \cos qz, \qquad f(z) = \frac{2}{L} \sum_q \eta_q f_q^p \cos qz \tag{5}$$

where

$$q = \left\{ \begin{array}{ll} \frac{2n\pi}{L}, & p = + \\ \frac{(2n+1)\pi}{L}, & p = - \end{array} \right\} \qquad n = 0, 1, 2, \ldots, \quad \eta_q = 1 - \frac{\delta_{q,0}}{2}.$$

Index p denotes that the q components of any quantity throughout this paper will have a well defined (even or odd) parity.

3. Spectral function

While bulk collective modes occur at frequencies for which the dielectric function equals zero, surface modes can be related to the dielectric function through equation [14, 4]:

$$S_p(\mathbf{Q}, \omega) = \frac{1}{\pi} \mathrm{Im} \frac{c_{-p}\varepsilon_p(\mathbf{Q}, \omega) - c_p}{\varepsilon_p(\mathbf{Q}, \omega) + 1} \qquad c_p = 1 - p\mathrm{e}^{-QL}. \tag{6}$$

Here $\varepsilon_p(\mathbf{Q}, \omega)$ is the surface dielectric function given by [2, 14, 4, 3]

$$\varepsilon_p^{-1}(\mathbf{Q}, \omega) = \frac{4Q}{L} \sum_{qq'} \left[\frac{8\pi e^2}{L} \chi^p_{qq'}(\mathbf{Q}, \omega) + (Q^2 + q^2) \frac{\delta_{qq'}}{\eta_q} \right]^{-1} \tag{7}$$

where the $\chi^p_{qq'}$ are the Fourier components of the irreducible polarizability. Replacing χ by the polarizability of the non-interacting electrons, (i.e. the Lindhard response function) leads to the RPA, but here we shall replace χ by χ^0, defined as

$$\chi^0(\mathbf{r}, \mathbf{r}', \omega) = \sum_{\nu,\nu'} \frac{f_\nu - f_{\nu'}}{E_\nu - E_{\nu'} - \hbar(\omega + \mathrm{i}\eta)} \Phi_\nu(\mathbf{r}) \Phi^*_{\nu'}(\mathbf{r}) \Phi_\nu(\mathbf{r}') \Phi^*_{\nu'}(\mathbf{r}') \tag{8}$$

with $f_\nu = 2\Theta(E_\mathrm{F} - E_\nu)$, where E_F is the Fermi energy, $\Theta(x)$ is the Heaviside function, η is a positive infinitesimal and Φ are the electron wavefunctions (3). In other words, if Φ were the free electron wavefunctions (8) would be the Lindhard response function, but if we use the Kohn–Sham wavefunctions instead, calculated with the effective potential that includes electron–electron interaction as well as exchange–correlation potential, it gets us beyond the RPA.

After Fourier transforming in the $\boldsymbol{\rho}$ direction, and denoting the highest occupied state with j_M, (8) can be written as [17]

$$\chi^0(\mathbf{Q}, z, z', \omega) = \sum_{j=1}^{j_M} \sum_{j'=1}^{\infty} F_{jj'}(\mathbf{Q}, \omega) \phi_j(z) \phi_{j'}(z) \phi_j(z') \phi_{j'}(z') \tag{9}$$

where $F_{jj'}(\mathbf{Q}, \omega)$ can be calculated analytically [4], and the result is

$$F_{jj'}(\mathbf{Q}, \omega) = \frac{-1}{\pi Q^2} \Big[2a_{jj'}(\mathbf{Q}) + \mathrm{sgn}(\omega - a_{jj'}(\mathbf{Q})) \sqrt{(\omega - a_{jj'}(\mathbf{Q}) + \mathrm{i}\eta)^2 - Q^2 k_j^2} - \mathrm{sgn}(\omega + a_{jj'}(\mathbf{Q})) \sqrt{(\omega + a_{jj'}(\mathbf{Q}) + \mathrm{i}\eta)^2 - Q^2 k_j^2} \Big] \tag{10}$$

where

$$a_{jj'}(\mathbf{Q}) = \frac{\hbar}{2m} Q^2 - \frac{\epsilon_j - \epsilon_{j'}}{\hbar}, \qquad k_j = \sqrt{\frac{2m}{\hbar}(E_\mathrm{F} - \epsilon_j)} \tag{11}$$

and ϵ_j is the 'perpendicular' energy defined in (4).

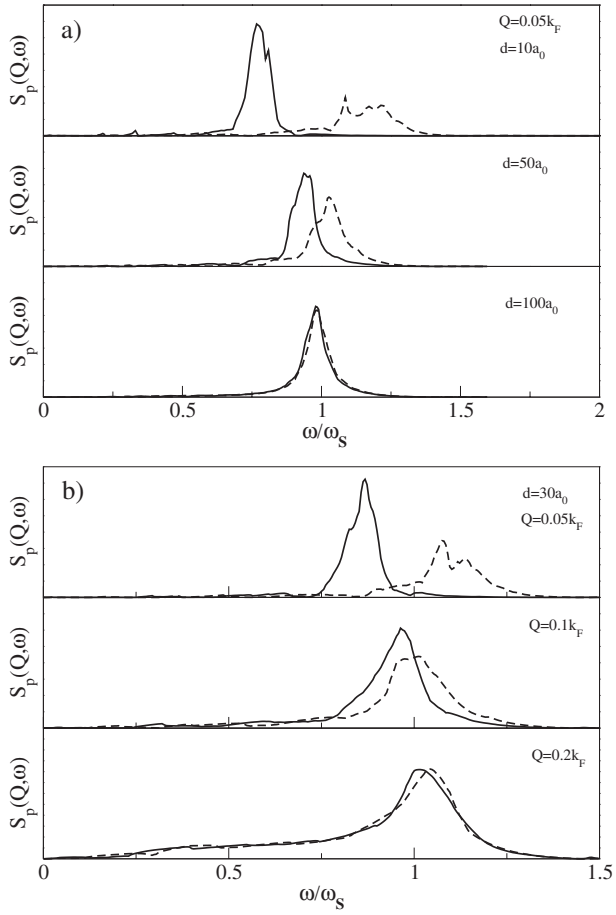

Figure 2. Examples of surface excitation spectra: (a) for wavevector $Q = 0.05k_F$ and different slab thicknesses d, (b) for thickness $d = 30a_0$ and different wavevectors Q. Full lines are for even modes, and dashed lines for odd modes.

4. Results and discussion

As described in the previous section, equation (6) together with equations (7)–(11) give the spectral functions of even and odd surface excitations in a metallic (jellium) slab. We performed calculations for $r_s = 2.07$ (where r_s is the radius defined by the electron density as $1/n = (4/3)\pi r_s^3$) which corresponds to aluminium, slab thicknesses from $d = 10a_0$ to $100a_0$ (with $a = 12a_0$, where a_0 is Bohr radius), for different values of Q varying from $0.01k_F$ to $0.2k_F$, and a few examples are shown in figure 2. The spectra are in agreement with the previously calculated ones [15, 16], and show the usual structure, though with the increase in precision one can observe some new features. On the other hand, our method enables us to distinguish various modes observed on these spectra from one another (odd from even, bulk from surface, single particle from collective), which is not easy when using other methods, so that we can analyse and interpret the spectra in much more detail.

Let us first discuss the collective modes. Figure 3 shows the wavevector dependence of the symmetric and antisymmetric surface plasmon peaks, for three different slab thicknesses.

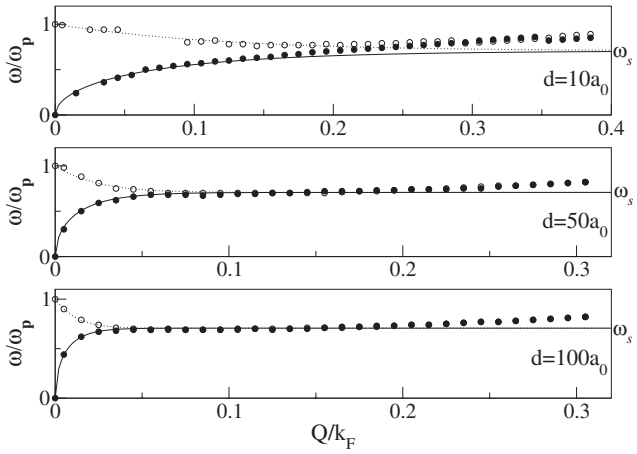

Figure 3. Dispersion relations of surface plasmons for different slab thicknesses $d = 10a_0$, $50a_0$, $100a_0$. Dots are for even modes, and circles for odd modes. The full and dotted lines represent the classical dispersions of even and odd plasmons, respectively.

Dots and circles represent the values obtained as the maximum values (most prominent peaks) of even and odd spectra calculated for each wavevector. For comparison we plotted the classical dispersion relations [18] for such a system (dotted and full lines represent even and odd branches respectively). In agreement with the result shown in figure 4 of [4], at large Q we observe the increase of both frequencies above the (classical) asymptotic SP frequency $\omega_s = \omega_p/\sqrt{2}$ (where $\omega_p = 4\pi ne^2/m$). That is also in agreement with the well known theoretical results for the dispersion of bulk plasmons and also surface plasmons in semi-infinite metals, and the measurements performed for such systems [19–22]. For small Q, the measured dispersion relation [19] decreases, as predicted theoretically [23], which neither agrees nor disagrees with our result since we study a slab of finite (and actually very small) thickness so the long-wavelength behaviour is predominantly defined by the geometry of the system, but for large Q it is in good agreement with our result.

In figure 4 we show the dependence of surface plasmon frequencies on the slab thickness for various values of the plasmon wavevector Q. As it is well known from the classical dispersion relations and from the calculated spectra [4, 8], for small Q, even and odd modes are further apart, while for large Q (approximately $Q \geqslant \frac{1}{L}$) they are closer and converge to a frequency slightly above the long-wavelength SP frequency ω_s. Our results show how, for wider slabs, surface plasmons actually behave very much like in a semi-infinite metal, i.e. the charge fluctuations on the two surfaces become decoupled. This, of course, is the expected result, but it is interesting to see that it happens for slabs less then 100 atomic units thick, and for slightly larger wavevectors ($Q > 0.05k_F$) even for slabs as thin as 50 au. The position of the surface plasmon shown in figure 5 for $Q = 0.05k_F$ strongly confirms this conclusion.

This is an interesting result because it implies, for example, that for the calculations of electron tunnelling between two semi-infinite metallic electrodes (which, for example, takes place in systems like an STM) we can simulate the semi-infinite electrode by a slab of finite (and in fact very small) thickness which is much more convenient for numerical calculations. For wider slabs we need more points for discretization of the variables z and z', but also the number of occupied energy levels increases, which means that the CPU time needed for such calculations does not increase linearly with the slab thickness $d = L - 2a$, but rather scales approximately as d^2. Since the calculation of the Kohn–Sham wavefunctions also becomes

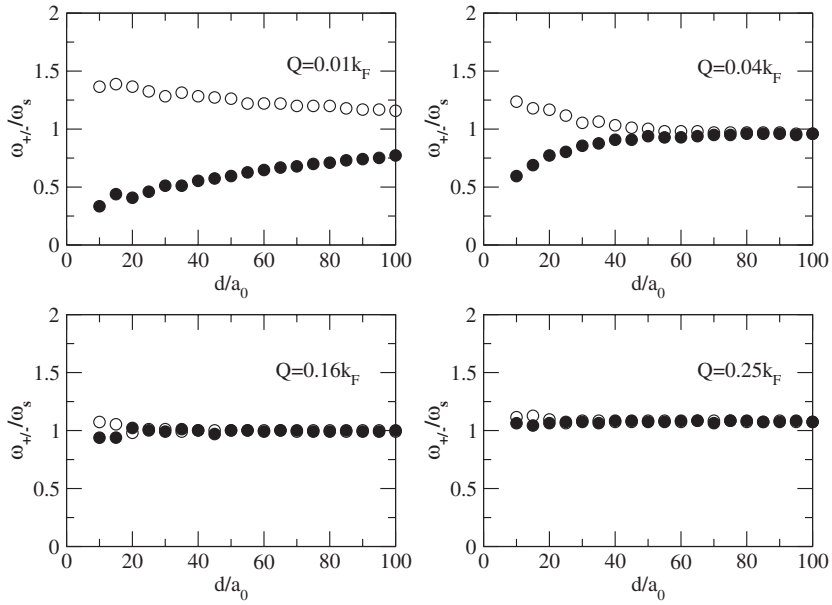

Figure 4. Collective mode frequencies against the slab thickness for various wavevectors. Dots are for even modes, and circles for odd modes.

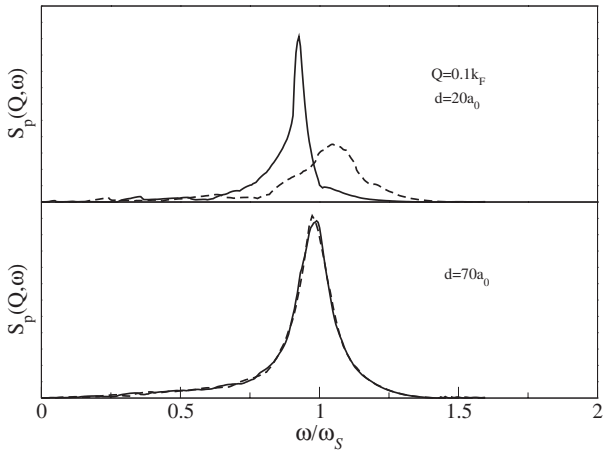

Figure 5. Surface plasmon peaks for $Q = 0.1k_{\mathrm{F}}$ and two thicknesses $d = 20a_0$ and $d = 70a_0$. Full lines are for even modes, and dashed lines for odd modes.

more time consuming for thicker slabs, it is clear that the numerical effort for the entire calculation depends tremendously on the slab thickness, and it is therefore very convenient to use thin slabs.

At lower frequencies below the surface plasmon peaks we observe the usual broad structures due to the continuum of intra-band electron–hole excitations, but on top of them we clearly observe (figures 5–7) some weak and quite periodic peaks. Trying to understand their origin, for example the possible relation to the electron resonances in the potential well (and therefore their dependence on the slab thickness), we first notice that intra-band transitions, for

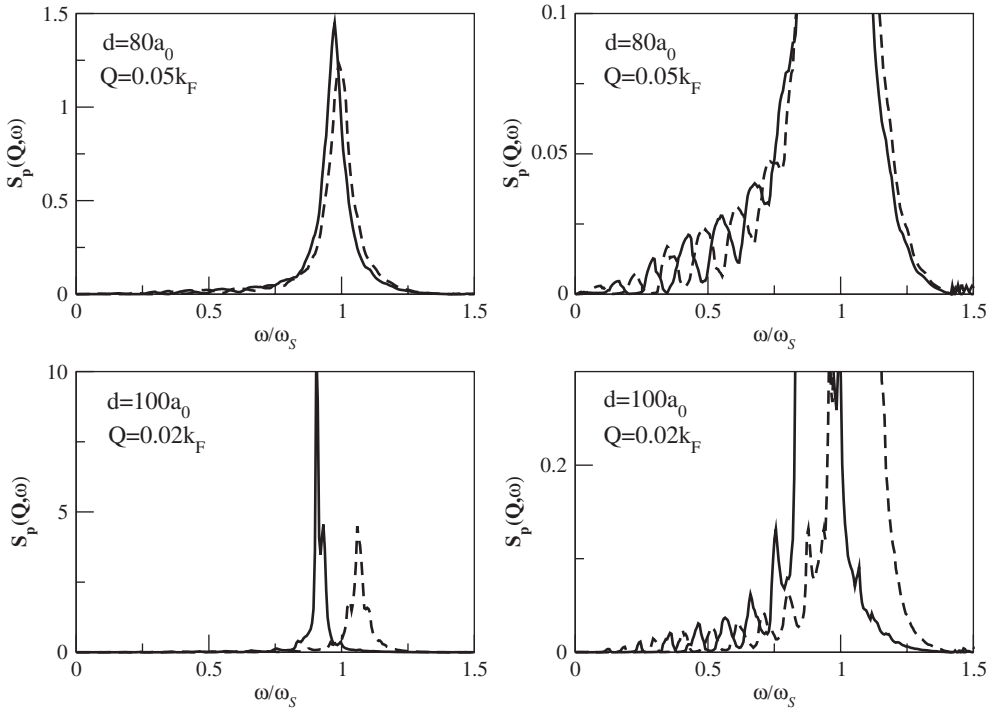

Figure 6. Surface plasmon spectra for $d = 80a_0$, $Q = 0.05k_F$ and $d = 100a_0$, $Q = 0.02k_F$. On the right-hand side the ordinates are rescaled to show the oscillations in the low-frequency parts of the spectra in detail. Full lines are for even modes, and dashed lines for odd modes.

a fixed wavevector Q, are possible for $0 < \omega < Qv_F + \frac{Q^2}{2m}$ (where v_F is the Fermi velocity), so above this region only inter-band transitions contribute. Analysing these oscillations in figure 6, we changed the scale on the ordinate to show the low-frequency parts of the spectra in detail, and we came to the conclusion that they are due to the electronic inter-band transitions (as schematically shown in figure 7).

In order to verify this, in figure 8 we show enlarged relevant parts of the calculated spectra $S_p(\mathbf{Q}, \omega)$ compared to the energy differences between the lowest unoccupied state and any of the occupied states, i.e. lines shown below each peak in the spectrum correspond to $\omega_j = \frac{E-E_j}{\hbar}$, where $j = 0, \ldots, j_M$, and E is the lowest eigenenergy above the Fermi level. Clearly, most of the peaks in the spectra are in very good agreement with the transition frequencies of corresponding parity. The rest of the peaks correspond either to intra-band transitions (small ω peaks) or to inter-band transitions to some higher unoccupied state (large ω peaks).

It could be interesting to analyse in more detail how the single-particle excitation spectrum, which is, in the absence of collective screening, given by

$$S_p^0(\mathbf{Q}, \omega) = -\frac{1}{\pi} \int \mathrm{d}z\, \mathrm{d}z' V_p\left(\mathbf{Q}, 0, z', \omega\right) \mathrm{Im}\, \chi^0\left(\mathbf{Q}, z, z', \omega\right) V_p\left(\mathbf{Q}, z', 0, \omega\right),$$

changes in the presence of the collective screening. In figure 9(a) we show calculated $S_p^0(\mathbf{Q}, \omega)$ which have extremely large values. This is obviously an unphysical result because $S_p^0(\mathbf{Q}, \omega)$ correspond to the situation in which the external field freely penetrates throughout the solid. In order to compare $S_p^0(\mathbf{Q}, \omega)$ with the fully screened $S_p(\mathbf{Q}, \omega)$ shown in figure 9(c), we can

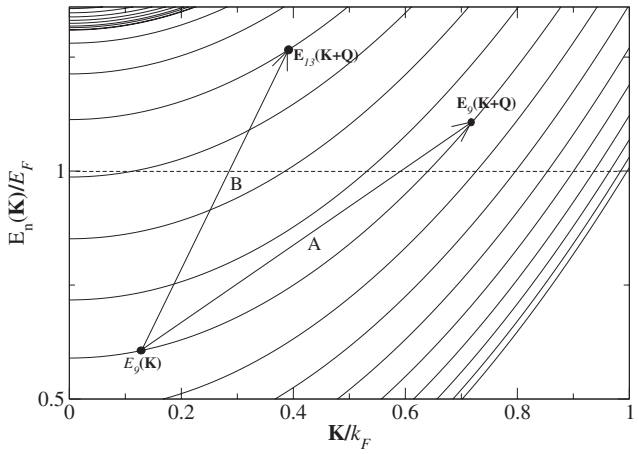

Figure 7. Energy scheme showing electronic intra-band (A), and inter-band (B) transitions in a jellium metallic slab.

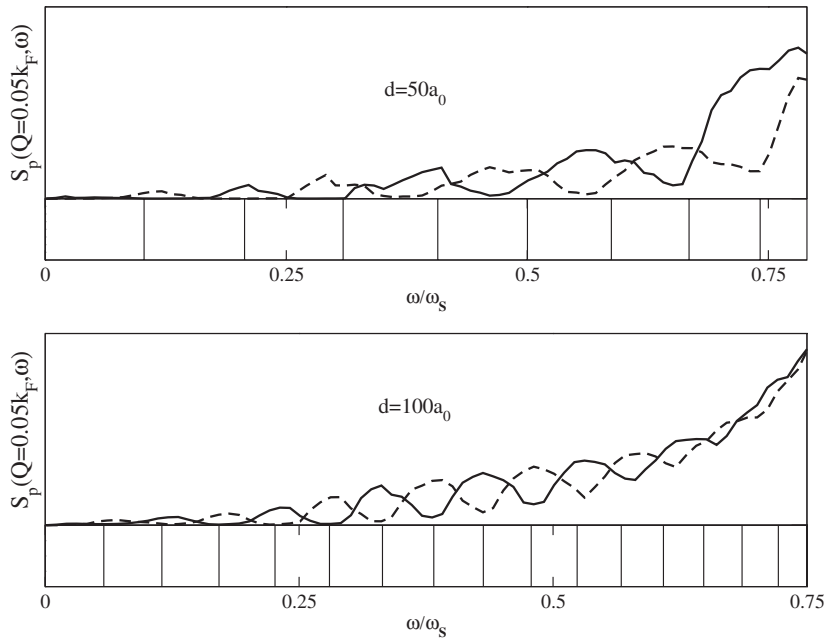

Figure 8. Details of surface excitation spectra showing single-particle excitations. The full line is for even excitations, and the dashed line for odd excitations.

approximate this reduction in intensity by dividing:

$$S_p^0 \to S_p^0/\left[\epsilon\left(\omega\right)+1\right].$$

For the local dielectric function $\epsilon(\omega) = 1 - \frac{\omega_p^2}{\omega^2}$ where ω_p is the bulk plasmon frequency, this gives the factor $\frac{\omega^2}{\omega_p^2}$, as shown in figure 9(b). We see that the single-particle peaks are located at the same frequencies for all three cases, but from figures 9(b) and (c) we can observe their modification due to the onset of the collective SP modes.

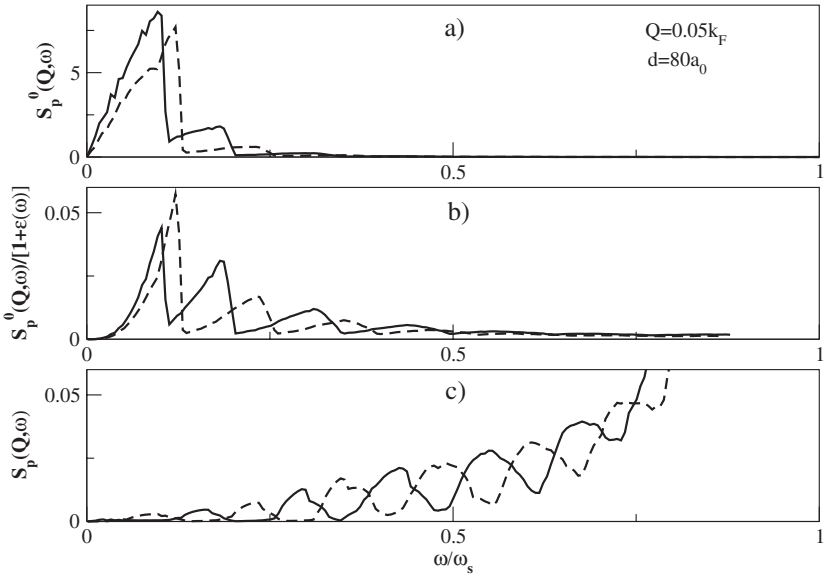

Figure 9. Modification of single-particle excitation structures, for $d = 80a_0$, $Q = 0.05k_F$, (a) unscreened spectrum $S_p^0(\mathbf{Q}, \omega)$; (b) unscreened spectrum reduced by the local dielectric function $\epsilon(\omega) + 1$; (c) fully screened spectrum $S_p(\mathbf{Q}, \omega)$.

5. Conclusions

Using the formalism developed in some earlier papers [4–8] and the method for the calculation of the Kohn–Sham wavefunctions described in [8], we have studied the details of the surface excitation spectra of metallic thin films, for various thicknesses. We examined both the collective and the single-particle parts of the spectra and found oscillatory structures that correspond to the inter-band transitions of metallic electrons. We also showed that collective surface excitations in slabs wider than 100 au (and for slightly larger plasmon wavevectors even wider than 50 au) already behave like those in the semi-infinite metal. With the exception of very small wavevectors (i.e. very long wavelengths), which is not that important from the point of view of numerical calculations since the long-wavelength limit can be treated analytically, knowing that very thin slabs can be used to model a semi-infinite metal is very important, because such systems require much less numerical effort.

References

[1] Lang N D and Kohn W 1970 *Phys. Rev.* B **1** 4555
[2] Newns D M 1970 *Phys. Rev.* B **1** 3304
[3] Marušić L and Šunjić M 1998 *Fizika* A **7** 145
[4] Marušić L and Šunjić M 2001 *Phys. Scr.* **63** 336
[5] Hohenberg P and Kohn W 1964 *Phys. Rev.* **136** B864
Kohn W and Sham L 1965 *Phys. Rev.* **140** A1133
[6] Eguiluz A G, Campbell D A, Maradudin A A and Wallis R F 1984 *Phys. Rev.* B **30** 5449
[7] Schulte F K 1976 *Surf. Sci.* **55** 427
[8] Despoja V, Marušić L and Šunjić M 2005 *Fizika* A **14** 207
[9] A review can be found e.g. in Payne M C, Teter M P, Allan D C, Arias T A and Joannopoulos J D 1992 *Rev. Mod. Phys.* **64** 1045
[10] Eguiluz A G, Heinrichsmeier M, Fletzar A and Hanke W 1992 *Phys. Rev. Lett.* **68** 1359

[11] Quong A A and Eguiluz A G 1993 *Phys. Rev. Lett.* **70** 3955
[12] Bergara A, Silkin V M, Chulkov E V and Echenique P M 2003 *Phys. Rev.* B **67** 245402
[13] Silkin V M, Chulkov E V and Echenique P M 2004 *Phys. Rev. Lett.* **93** 176801
[14] Penzar Z and Šunjić M 1984 *Phys. Scr.* **30** 431
Penzar Z and Šunjić M 1983 *Solid State Commun.* **46** 385
[15] Eguiluz A G 1983 *Phys. Rev. Lett.* **51** 1907
[16] Schaich W L and Dobson J F 1994 *Phys. Rev.* B **49** 14700
[17] Eguiluz A G 1985 *Phys. Rev.* B **31** 3303
[18] Ritchie R H 1957 *Phys. Rev.* **106** 874
[19] Tsuei K D, Plummer E W and Feibelman P J 1989 *Phys. Rev. Lett.* **63** 2256
[20] Suto S, Tsuei K D and Plummer E W 1989 *Phys. Rev. Lett.* **63** 2590
[21] Rocca M, Lazzarino M and Valbusa U 1992 *Phys. Rev. Lett.* **69** 2122
Savio L, Vattuone L and Rocca M 2000 *Phys. Rev.* B **61** 7324
Chiarello G, Formoso V, Santinello A, Colavita E and Papagno L 2000 *Phys. Rev.* B **62** 12676
[22] A review can be found e.g. in Plummer E W, Tsuei K D and Kim B-O 1995 *Nucl. Instrum. Methods* B **96** 448
[23] Feibelman P J 1973 *Phys. Rev. Lett.* **30** 975
Feibelman P J 1989 *Phys. Rev.* B **40** 2752
Feibelman P J and Tsuei K D 1990 *Phys. Rev.* B **41** 8519